Exploring Features in a Bayesian Framework for Material Recognition

Ce Liu[1,3] Lavanya Sharan[2,3] Edward H. Adelson[3] Ruth Rosenholtz[3]
[1]Microsoft Research New England [2]Disney Research Pittsburgh [3]Massachusetts Institute of Technology
celiu@microsoft.com {lavanya,adelson,rruth}@csail.mit.edu

Abstract

We are interested in identifying the material category, e.g. glass, metal, fabric, plastic or wood, from a single image of a surface. Unlike other visual recognition tasks in computer vision, it is difficult to find good, reliable features that can tell material categories apart. Our strategy is to use a rich set of low and mid-level features that capture various aspects of material appearance. We propose an augmented Latent Dirichlet Allocation (aLDA) model to combine these features under a Bayesian generative framework and learn an optimal combination of features. Experimental results show that our system performs material recognition reasonably well on a challenging material database, outperforming state-of-the-art material/texture recognition systems.

1. Introduction

Material recognition is an important aspect of visual recognition. We interact with a variety of materials on a daily basis and we constantly assess their appearance. For example, when judging where to step on an icy sidewalk or buying fresh produce at a farmers' market or deciding whether a rash requires a trip to the doctor, material qualities influence our decisions. Therefore, it is valuable to build a visual recognition system that can infer material properties from images.

The problem of recognizing materials from photographs has been addressed mainly in the context of reflectance estimation. The visual appearance of a surface depends on several factors – the illumination conditions, the geometric structure of the surface sample at several spatial scales, and the surface reflectance properties, often characterized by the bidirectional reflectance distribution function (BRDF) [24] and its variants [9, 16, 26]. A number of techniques have been developed that can estimate the parameters of a BRDF model from a set of photographs, under restrictive assumptions of illumination, geometry and material properties [10, 11].

In this paper, we focus on recognizing high-level material categories, such as glass, metal, fabric, plastic or wood, instead of explicitly estimating reflectance properties. The reflectance properties of a material are often correlated with its high-level category (e.g. glass is usually translucent and wood is often brown), and in this work, we will exploit these correlations. However, it is important to point out that knowing only the reflectance properties of a surface is not sufficient for determining the material category. For example, the fact that a surface is translucent does not tell us if it is made of plastic, wax or glass.

Figure 1. **Material recognition in the wild.** The goal of this paper is to learn to recognize material categories from a single image. For this purpose, we will use our Flickr Materials Database [28] that captures a range of appearances within each material category.

Unlike other visual recognition tasks such as object or texture recognition, it is challenging to find good features that can distinguish different material categories because of the wide variations in appearance that a material can display. Our strategy is to design several low-level and middle-level features to characterize various aspects of material appearance. In addition to well-established features such as color, jet and SIFT [17, 21], we introduce several new features, such as curvature of edges, histogram of oriented gradient (HOG) feature along edges, and HOG perpendicular

Figure 2. **Material recognition vs. object recognition**. These vehicles are made of different materials (from left to right): *metal*, *plastic* and *wood*.

Figure 3. **Material recognition vs. texture recognition**. These checkerboard patterns are made of different materials (left to right): *fabric*, *plastic* and *paper*.

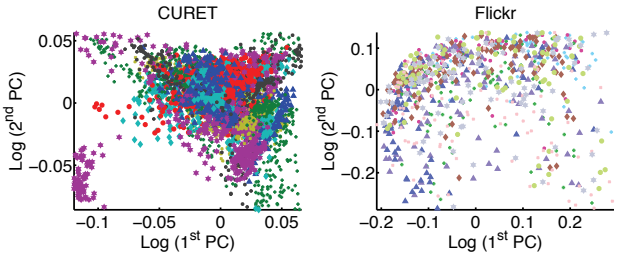

Figure 4. The projection on the first two principal components (PCs) of the texton histograms are shown for all images in the (left) 61 classes in the CURET database [9] and (right) 10 classes in the Flickr Materials Database [28]. The textons were derived from 5×5 pixel patches, as described in [30]. The colors indicate the various texture/material categories. CURET samples are more separable than Flickr.

to edges. After quantizing these features into dictionaries, we convert an image into a bag of words and use latent Dirichlet allocation (LDA) [3] to model the distribution of the words. By allowing topics to be shared amongst material categories, LDA is able to learn clusters of visual words that characterize different materials. We call our model augmented LDA (aLDA) as we concatenate dictionaries from various features and learn the optimal combination of the features by maximizing the recognition rate.

It is crucial to choose the right image database to evaluate our system. Most existing material/texture image databases fail to capture the complexity of real world materials, because they are either instance databases, such as CURET [9], or texture category databases with very few samples per class, such as KTH-TIPS2 [5]. The high recognition rates achieved on these databases ($> 95\%$ on CURET [30]) suggests a need for challenging, real world material databases.

In this work, we use the Flickr Materials Database [28] created by us, originally for studying the visual perception of materials. This database contains 10 common material categories - *fabric*, *foliage*, *glass*, *leather*, *metal*, *paper*, *plastic*, *stone*, *water* and *wood* (see Figure 1). We acquired 100 color photographs from Flickr.com for each category, including 50 close-ups and 50 object-level views. All images have 512×384 pixel resolution and contain a single material category in the foreground. These images capture a wide range of appearances within each material category. We show that although material categorization can be a very challenging problem, especially on a database like ours, our system performs reasonably well, outperforming state-of-the-art systems such as [30].

2. Related Work

Recognizing high-level material categories in images is distinct from the well-studied problem of object recognition. Although object identity is sometimes predictive of material category, a given class of objects can be made of different materials (see Figure 2) and different classes of objects can be made of the same material (see Figure 1). Therefore, many recent advances in object recognition such as shape context [2], object detectors [7] and label transfer [19] may not be applicable for material recognition. In fact, most object recognition systems rely on material-invariant features and tend to ignore material information altogether.

Material recognition is closely related to, but different from, texture recognition. Texture has been defined in terms of dimensions like periodicity, orientedness, and randomness [20]. It can be an important component of material appearance, *e.g.* wood tends to have textures distinct from those of polished metal. However, as illustrated in Figure 3, surfaces made of different materials can share the same texture patterns and as a consequence, mechanisms designed for texture recognition [18, 30] may not be ideal for material recognition.

Material recognition is also different from BRDF estimation. In computer graphics, there is great interest in capturing the appearance of real world materials. The visual appearance of materials like wood or skin, has been modeled in terms of the bidirectional reflectance distribution function (BRDF) [10, 22] and related representations such as BTF [9] and BSSRDF [16]. Material recognition might seem trivial if the BRDF is known, but in general, it is nearly impossible to estimate the BRDF from a single image without simplifying assumptions [10, 11].

A number of low-level image features have been developed for identifying materials. The shape of the luminance histogram of images was found to correlate with human judgement of surface albedo [25], and was used to classify images of spheres as shiny, matte, white, grey *etc*. [11]. Similar statistics were used to estimate the albedo and gloss of stucco-like surfaces [27]. Several techniques have been developed to search for specific materials in real world photographs such as glass [15, 23] or skin [14].

The choice of databases is, often, the key to success in vi-

sual recognition. The CURET database [9] that consists of images of 61 different texture samples under 205 different viewing and lighting conditions, has become the standard for evaluating 3-D texture classification algorithms. A variety of methods based on texton representations [6, 18, 29], bidirectional histograms [8] and image patches [30] have been successful at classifying CURET surfaces ($> 95\%$ accuracy). The KTH-TIPS2 database [5] consisting of 11 texture categories, 4 samples per category, and each photographed under a variety of conditions, was introduced to increase the intra-class variation. It was shown that a SVM-based classifier achieves 98.5% accuracy on this database [5]. Our Flickr Materials Database [28] contains 10 material categories and 100 diverse samples in category. On inspecting the images in Figure 1 and the plots in Figure 4, it is apparent that the Flickr Materials Database is more challenging than the CURET database, and for this reason we chose the Flickr Materials Database to develop and evaluate our material recognition system.

3. Features for Material Recognition

In order to build a material recognition system, it is important to identify features that can distinguish material categories from one another. What makes metal look like metal and wood look like wood? Is it color (neutral vs. browns), textures (smooth vs. grainy) or reflectance properties (shiny vs. matte)? Since little is known about which features are suited for material recognition, our approach is to try a variety of features, some borrowed from the fields of object and texture recognition, and some new ones developed specifically for material recognition. From a rendering point of view, once the camera and the object are fixed, the image of the object can be determined by (i) the BRDF of the surface, (ii) surface structures, (iii) object shape and (iv) environment lighting. Given the diversity of appearance in the Flickr Materials Database, we will attempt to incorporate all these factors in our features.

(a) Color and Texture

Color is an important attribute of surfaces and can be a cue for material recognition: wooden objects tend to be brown, leaves are green, fabrics and plastics tend to be saturated with vivid color, whereas stones tend to be less saturated. We extract 3×3 pixel patches from an RGB image as our color feature.

Texture, both of the wallpaper and 3-D kind [26], can be useful for distinguishing materials. For example, wood and stone have signature textures that can easily tell them apart. We use two sets of features to measure texture. The first set comprises the filter responses of an image through a set of multi-scale, multi-orientation Gabor filters, often called filter banks or **jet** [17]. Jet features have been used to recognize 3-D textures [18, 30] by clustering to form *textons* and using the distribution of textons as a feature. The second set

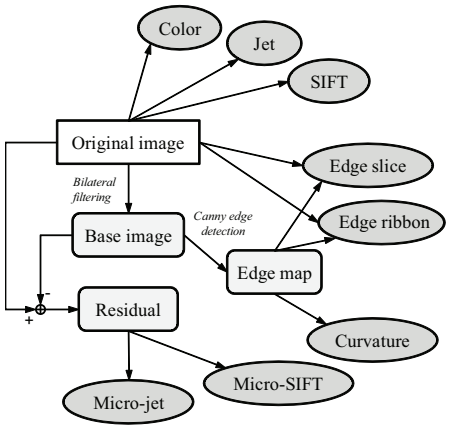

Figure 5. Illustration of how our system generates features.

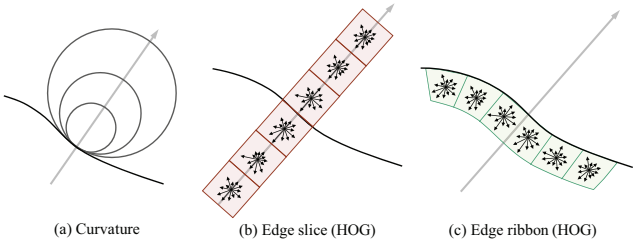

(a) Curvature (b) Edge slice (HOG) (c) Edge ribbon (HOG)

Figure 6. We extract *curvature* at three scales, *edge slice* in 6 cells, and *edge ribbon* in 6 cells at edges.

of features we use is **SIFT** [21]. SIFT features have been widely used in scene and object recognition to characterize the spatial and orientational distribution of local gradients [13].

(b) Micro-texture

Two surfaces sharing the same BRDF can look different if they have different surface structures, *e.g.* if one is smooth and the other is rough. In practice, we usually touch a surface to sense how rough (or smooth) it is. However, our visual system is able to perceive these properties even without a haptic input. For example, we can see tiny hairs on fabric, smooth surfaces in glass objects, crinkles in leather and grains in paper.

In order to extract information about surface structure, we followed the idea in [1], of smoothing an image by bilateral filtering [12] and then using the residual image for further analysis. The process is illustrated in Figure 7. We choose three images from material categories (a) - glass, metal and fabric - and perform bilateral filtering to obtain base image in (b) and display the residual in (d). The residual of bilateral filtering reveals variations in pixel intensity at a finer scale. For the fabric and metal example in Figure 7, the residual is due to surface structure whereas for glass, these variations are related to translucency. Although it is hard to cleanly separate the contributions of surface structure from those of the BRDF, the residual contains useful information about material category. We apply the same approach for characterizing the residual as we did for texture.

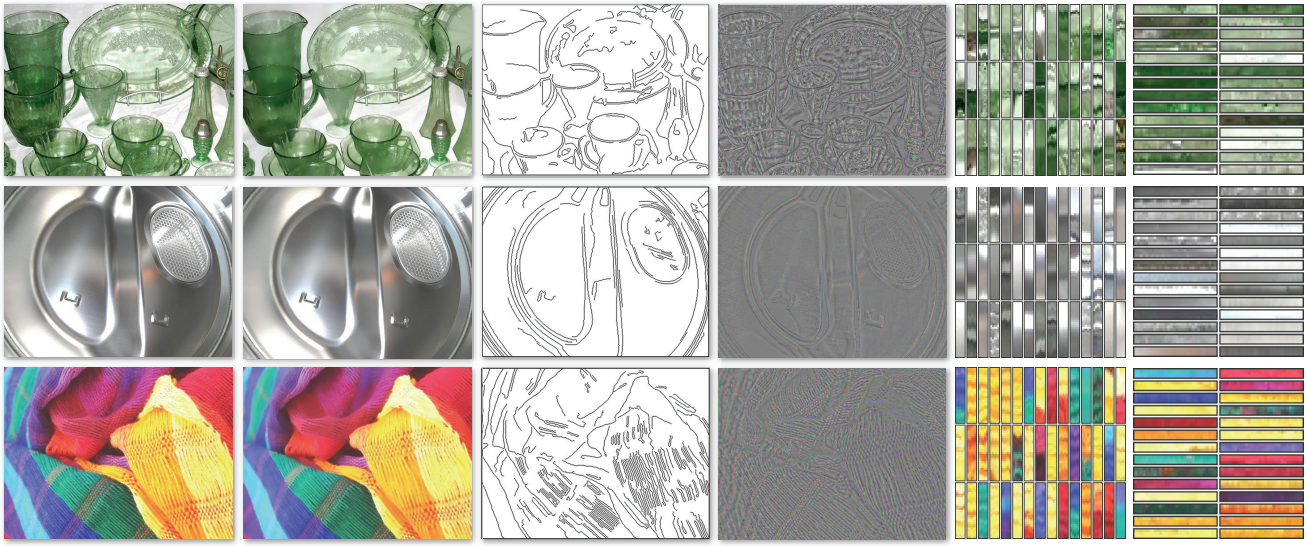

(a) Original image (b) Base image (bilateral filtering) (c) Canny edges on (b) (d) Residual image: (a)-(b) (e) Edge slices (f) Edge ribbon

Figure 7. **Some features for material recognition**. From top to bottom is *glass*, *metal* and *fabric*. For an image (a) we apply bilateral filtering [1] to obtain the base image (b). We run Canny edge detector [4] on the base image and obtain edge maps (c). *Curvatures* of the edges are extracted as features. Subtracting (b) from (a), we get the residual image (d) that shows micro structures of the material. We extract *micro-jet* and *micro-SIFT* features on (d) to characterize material micro-surface structure. In (e), we also show some random samples of edge slices along the normal directions of the Canny edges. These samples reveal lighting-dependent features such as specular highlights. The edge ribbon samples are shown in (f). Arrays of HOG's [7] are extracted from (e) and (f) to form *edge-slice* and *edge-ribbon* features.

We compute the jet and SIFT features of the residual image, and name them **micro-jet** and **micro-SIFT** for clarity.

(c) Outline Shape

Though a material can be cast into any arbitrary shape, the outline shape of a surface and its material category are often related *e.g*. fabrics and glass have long, curved edges, while metals have straight lines and sharp corners. The outline shape of a surface can be captured by an edge map. We run the Canny edge detector [4] on the base image, trim out short edges, and obtain the edge map shown in Figure 7 (c). To characterize the variations in the edge maps across material categories, we measured the **curvature** on the edge map at three different scales as a feature (see Figure 6).

(d) Reflectance-based features

Glossiness and transparency are important cues for material recognition. Metals are mostly shiny, whereas wooden surfaces are usually dull. Glass and water are translucent, while stones are often opaque. These reflectance properties sometimes manifest as distinctive intensity changes at the edges in an image. To measure these changes, as shown in Figure 6 (b), we extract histogram of oriented gradients (HOG) [7] features along the *normal* direction of edges. We take a slice of pixels with a certain width along the normal direction, compute the gradient at each pixel, divide the slice into 6 cells, and quantize the oriented gradients in to 12 angular bins. This feature is called **edge-slice**. We also measure how the images change along the *tangent* direction of the edges in a similar manner, as suggested in Figure 6 (c). This feature is called **edge-ribbon**, which is also quantized by 6 cells and 12 angular bins for each cell.

We have described a pool of features that can be potentially useful for material recognition: **color**, **SIFT**, **jet**, **micro-SIFT**, **micro-jet**, **curvature**, **edge-slice** and **edge-ribbon**. The flowchart of how our system generates these features is shown in Figure 5. Amongst these features, color, SIFT and jet are *low-level* features directly computed from the original image and they are often used for texture analysis. The rest of the features, micro-SIFT, micro-jet, curvature, edge-slice and edge-ribbon are *mid-level* features that rely on estimations of base images and edge maps (Figures 7 (b) & (c)). A priori, we do not know which of these features will perform well. Hence, we designed a Bayesian learning framework to select best combination of features.

4. A Bayesian Computational Framework

Now that we have a pool of features, we want to combine them to build an effective material recognition system. We quantize the features into visual words and extend the LDA [3] framework to select good features and learn per-class distributions for recognition.

4.1. Feature quantization and concatenation

We use the standard k-means algorithm to cluster the instances of each feature to form dictionaries and map image

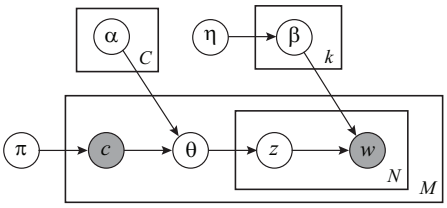

Figure 8. The graphical model of LDA [3]. Notice that our categorization shares both the topics and codewords. Different from [13], we impose a prior on β to account for insufficient data.

features into visual words. Suppose there are m features in the feature pool and m corresponding dictionaries $\{D_i\}_{i=1}^m$. Each dictionary has V_i codewords, *i.e.* $|D_i|=V_i$. Since features are quantized separately, the words generated by the ith feature are $\{w_1^{(i)},\cdots,w_{N_i}^{(i)}\}$, $w_j^{(i)}\in\{1,2,\cdots,V_i\}$ and N_i is the number of words. In order to put a set of different words together, a document of m sets of words

$$\{w_1^{(1)},\cdots,w_{N_1}^{(1)}\},\{w_1^{(2)},\cdots,w_{N_2}^{(2)}\},\cdots,\\ \{w_1^{(m)},\cdots,w_{N_m}^{(m)}\} \quad (1)$$

can be augmented to one set

$$\{w_1^{(1)},\cdots,w_{N_1}^{(1)},w_1^{(2)}+V_1,\cdots,w_{N_2}^{(2)}+V_1,\cdots,\\ w_1^{(m)}+\textstyle\sum_{i=1}^{m-1}V_i,\cdots,w_{N_m}^{(m)}+\sum_{i=1}^{m-1}V_i\} \quad (2)$$

with a joint dictionary $\mathbb{D}=\cup_i D_i,\ |\mathbb{D}|=\sum_{i=1}^m V_i$. In this way, we reduced the multi-dictionary problem to a single-dictionary one.

4.2. Latent Dirichlet Allocation

The latent Dirichlet allocation (LDA) [3] was invented to model the hierarchical structures of words. Details of the model can be found in [3, 13]. In order to be self-contained, we will briefly describe the model in the context of material recognition. As depicted in the graphical model in Figure 8, we first randomly draw the material category $c\sim\mathrm{Mult}(c|\pi)$ where $\mathrm{Mult}(\cdot|\pi)$ is a multinomial distribution with parameter π. Based on c, we select a hyper-parameter α_c, based on which we draw $\theta\sim\mathrm{Dir}(\theta|\alpha_c)$ where $\mathrm{Dir}(\cdot|\alpha_c)$ is a Dirichlet distribution with parameter α_c. θ has the following property: $\sum_{i=1}^k\theta_i=1$ where k is the number of elements in θ. From θ we can draw a series of topics $z_n\sim\mathrm{Mult}(z|\theta), n=1,\cdots,N$. The topic $z_n(=1,\cdots,k)$ selects a multinomial distribution β_{z_n} from which we draw a word $w_n\sim\mathrm{Mult}(w_n|\beta_{z_n})$, which corresponds to a quantization cluster of the features. Unlike [13] where β is assumed to be a parameter, we impose a conjugate prior η upon β to account for insufficient data as suggested by [3].

Since it is intractable to compute the log likelihood $\log p(w|\alpha_c,\eta)$, we instead maximize the lower bound $\mathcal{L}(\alpha_c,\eta)$ estimated through the variational distributions over $\theta,\{z_d\},\beta$. Please refer to [3] for details on deriving the variational lower-bound and parameter learning for α and η. Once we have learned α_c and η, we can use Bayesian MAP criterion to choose the material category

$$c^*=\arg\max_c\mathcal{L}(\alpha_c,\eta)+\lambda_c. \quad (3)$$

where $\lambda_c=\log\pi_c$.

4.3. Prior learning

A uniform distribution is often assumed for the prior $p(c)$, *i.e.* each material category will appear equally. However, since we learn the LDA model for each category independently (only sharing the same β), the learning procedure may not converge in finite iterations. Therefore, the probability density functions (pdfs) should be grounded for a fair comparison. We designed the following greedy algorithm to learn λ by maximizing the recognition rate (or minimizing the error).

Suppose $\{\lambda_i\}_{i\neq c}$ is fixed and we want to optimize λ_c to maximize the rate. Let y_d be the label for document d. Let $q_{d,i}=\mathcal{L}_d(\alpha_i,\eta)+\lambda_i$ be the "log posterior" for document d to belong to category i. Let $f_d=\max_i q_{d,i}$ be the maximum posterior for document d. We define two sets:

$$\begin{aligned}\Omega_c &= \{d|y_d=c,\ f_d>q_{d,c}\},\\ \Phi_c &= \{d|y_d\neq c,\ f_d=q_{d,y_d}\}.\end{aligned} \quad (4)$$

Set Ω_c includes the documents that are labeled as c and misclassified. Set Φ_c includes the documents that are not labeled as c and correctly classified. Our goal is to choose λ_c to make $|\Omega_c|$ as small as possible and $|\Phi_c|$ as large as possible. Notice that if we increase λ_c, then $|\Omega_c|\downarrow$ and $|\Phi_c|\downarrow$, therefore the optimal λ_c exists. We define the set of correctly classified documents with λ_c's

$$\begin{aligned}\Psi_c &= \{d|d\in\Omega_c,\ f_d<q_{d,c}+\lambda_c'-\lambda_c\}\cup\\ &\quad\{d|d\in\Phi_c,\ f_d>q_{d,c}+\lambda_c'-\lambda_c\},\end{aligned} \quad (5)$$

and choose the new λ_c that maximizes the size of Ψ_c:

$$\lambda_c\leftarrow\arg\max_{\lambda_c'}|\Psi_c|. \quad (6)$$

We iterate this procedure for each c repeatedly until each λ_c does not change.

4.4. Augmented LDA (aLDA)

Shall we use all the features in our predefined feature pool? Do more features imply better performance? Unfortunately, this is not true as we have limited training data. The more features we use, the more likely that the model overfits the training data and the performance decreases on test set. We designed a greedy algorithm in Figure 9 to select an optimal subset of our feature pool. The main idea is to select the best feature, one at a time, that maximizes the recognition rate on an evaluation set. The algorithm stops when adding more features will decrease the recognition rate. Note that we randomly split the training set H into L for parameter learning and E for cross evaluation. After $\mathbb{D}$ is learned, we use the entire training set H to relearn the parameters for $\mathbb{D}$.

Input: dictionary pool $\{D_1, \cdots, D_m\}$, training set H

- Initialize: $\mathbb{D} = \emptyset$, recognition rate $r = 0$
- Randomly split $H = L \cup E$

  for $l = 1$ to m

    for $D_i \notin \mathbb{D}$

      - Augment dictionary $\mathbb{D}' = \mathbb{D} \cup \{D_i\}$
      - Concatenate words according to $\mathbb{D}'$ using Eqn. (2)
      - Train LDA on L for each category (sharing β)
      - Learn prior λ using Eqn. (5) and (6)
      - r_i = recognition rate on E using Eqn. (3)

    end

    if $\max r_i > r$

      - $j = \arg\max_i r_i, \mathbb{D} = \mathbb{D} \cup \{D_j\}, \ r = r_j$

    else

      break

    end

  end

- Train LDA and learn prior λ on H
- r = recognition rate on H

Output: $\mathbb{D}, \ r$

Figure 9. **The augmented LDA (aLDA) algorithm**.

5. Experimental Results

We used the Flickr Materials Database [28] for all experiments described in this paper. There are ten material categories in the database: *fabric*, *foliage*, *glass*, *leather*, *metal*, *paper*, *plastic*, *stone*, *water* and *wood*. Each category contains 100 images, 50 of which are close-up views and the rest 50 are of views at object-scale (see Figure 1). There is a binary, human-labeled mask associated with each image describing the location of the object. We only consider pixels inside this binary mask for material recognition and disregard all the background pixels. For each category, we randomly chose 50 images for training and 50 images for test. All the experimental results reported in this paper are based on the same split of training and test.

We extract features for each image according to Figure 5. Mindful of computational costs, we sampled *color*, *jet*, *SIFT*, *micro-jet* and *micro-SIFT* features on a coarse grid (every 5^{th} pixel in both horizontal and vertical directions). Because there are far fewer pixels in edge maps than in the original images, we sampled every other edge pixel for *curvature*, *edge-slice* and *edge-ribbon*. Once features are extracted, they are clustered separately using k-means according to the number of clusters in Table 1. We specified the number of clusters for each feature, considering both dimensionality and the number of instances per feature.

After forming the dictionaries for each feature, we run the aLDA algorithm to select features incrementally. When learning the optimal feature set, we randomly split the 50 training images per category (set H) to 30 for estimating parameters (set L) and 20 for evaluation (set E). After the feature set is learned, we re-learn the parameters using the 50 training images per category and report the training/test rate. In the LDA learning step, we vary the number of topics from 50 to 250 with step size 50 and pick the best one. The learning procedure is shown in Figure 10, where for each material category we plot the training rate on the left in a darker color and test rate on the right in a lighter color. In Figure 10, the recognition rate is computed on the entire training/test set, not just on the learning/evaluation set. First, the system tries every single feature and discovers that amongst all features, SIFT produces the highest evaluation rate. In the next iteration, the system picks up color from the remaining features, and then edge-slice. Including more features causes the performance to drop and the algorithm in Figure 9 stops. For this final feature set "color + SIFT + edge-slice", the training rate is 49.4% and the test rate is 44.6%. The recognition rate of random guesses is 10%.

The boost in performance from the single best feature (SIFT, 35.4%) to the best feature set (color + SIFT + edge-slice, 44.6%) is due to our aLDA model that augments visual words. Interestingly, augmenting more features decreases the overall performance. When we use all the features, the test rate is 38.8%, lower than using fewer features. More features creates room for overfitting, and one solution to combat overfitting is to increase the size of the database. The fact that SIFT is the best-performing single feature in-

Feature name	Dim	average # per image	# of clusters
Color	27	6326.0	150
Jet	64	6370.0	200
SIFT	128	6033.4	250
Micro-jet	64	6370.0	200
Micro-SIFT	128	6033.4	250
Curvature	3	3759.8	100
Edge-slice	72	2461.3	200
Edge-ribbon	72	3068.6	200

Table 1. The dimension, number of clusters and average number per image for each feature.

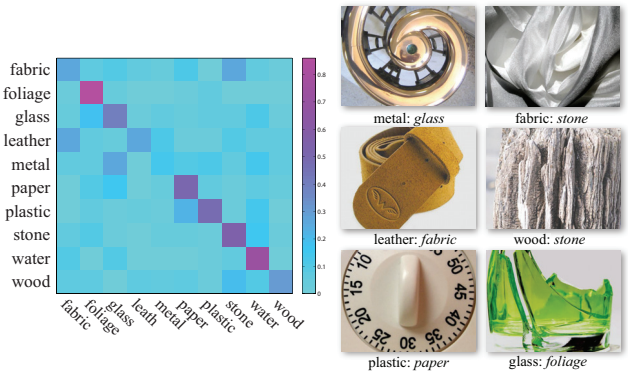

Figure 12. Left: the confusion matrix of our material recognition system using color + SIFT + edge-slice feature set. Row k is the probability distribution of class k being classified to each category. Right: some misclassification examples. Label "metal: *glass*" means that a metal material is misclassified as glass.

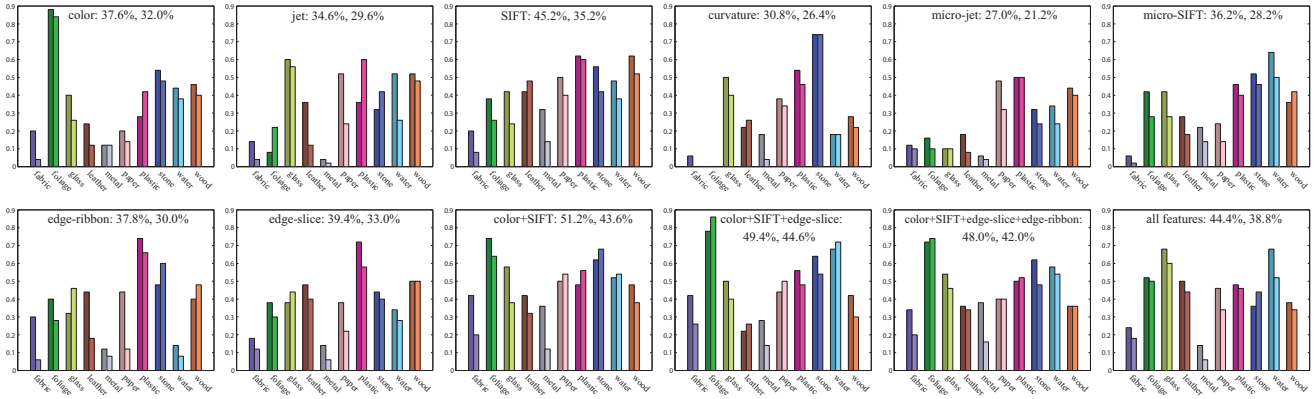

Figure 10. **The per-class recognition rate (both training and test) with different sets of features for the Flickr database** [28]. In each plot, the left, darker bar means training, the right, lighter bar means test. For the two numbers right after the feature set label are the recognition rate on the entire training set and the rate on the entire test set. For example, "color: 37.6%, 32.0%" means that the training rate is 37.6% and the test rate is 32.0%. Our aLDA algorithm finds "color + SIFT + edge-slice" to be the optimal feature set on the Flickr Materials Database.

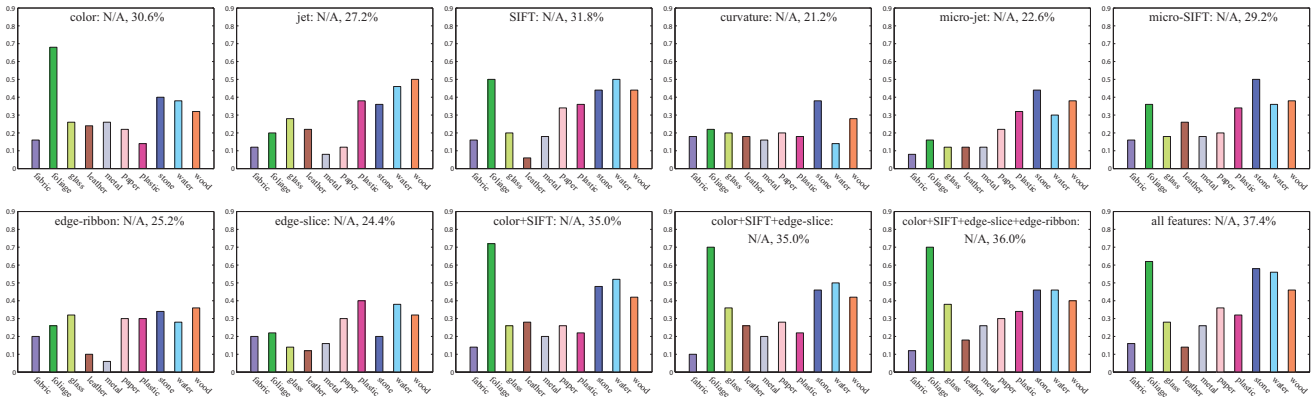

Figure 11. For comparison, we run Varma-Zisserman's system [30] (nearest neighbor classifiers using histograms of visual words) on our feature sets. Because of the nearest neighbor classifier, the training rate is always 100%, so we simply put it as N/A.

dicates the importance of texture in material recognition. In addition, SIFT also encapsulates some of the information captured by micro-SIFT. Edge-slice, which measures reflectance features, is also useful.

For comparison, we implemented and tested Varma-Zisserman's (VZ) algorithm [30] on the Flickr Materials Database. The VZ algorithm clusters 5×5 pixel gray-scale patches as codewords, obtains a histogram of the codewords for each image, and performs recognition using a nearest neighbor classifier. As a sanity check, we ran our implementation of VZ on the CURET database and obtained 96.1% test rate (their numbers are $95 \sim 98\%$, [30]). Next, we ran the exact VZ system tested on CURET on the Flickr Materials Database. The VZ test rate is 23.8%. This supports the conclusions from Figure 4 that the Flickr Materials Database is much harder than the CURET texture database.

As the VZ system uses features tailored for the CURET database (5×5 pixel patches), we ran VZ's algorithm using our features on Flickr Materials Database. The results of running VZ's system on exactly the same feature sets as in Figure 10 are listed in Figure 11. Since VZ uses a nearest neighbor classifier, it is meaningless to report the training rate as it is always 100%, so we only report the test rate. It is obvious why many of our features outperform fixed size gray-scale patch features on Flickr Materials Datatbase. In fact, the VZ system running on SIFT features has test rate of 31.8%, close to our system using SIFT alone (35.2%). However, combining features under the VZ's framework only slightly increases the performance to a maximum of 37.4%. Clearly, the aLDA model contributes to the boost in performance from 37.4% to 44.6%.

The confusion matrix of our system (color + SIFT + edge-slice, test rate 44.6%) in Figure 12 tells us how often each category is misclassified as another. For example, *fabric* is often misclassified as *stone*, *leather* misclassified as *fabric*, *plastic* misclassified as *paper*. The category *metal* is more likely to be classified as *glass* than itself. Some misclassification examples are shown in Figure 12. These results are not surprising because there are certain commonalities between *leather* and *fabric*, *plastic* and *paper*, as well

as *metal* and glass, as shown in Figure 12.

6. Discussion and Conclusion

Although the recognition rate achieved by our system 44.6% is lower than the rates reported in object recognition (*e.g.* [19]), it is significantly higher than the state of the art (23.8%, [30]). As illustrated in Figures 1 and 4, the sheer diversity and range of the Flickr Materials Database makes it a challenging benchmark for material recognition. We believe that material recognition is an important problem to study, and in this paper, we are merely taking one of the first steps towards understanding the problem.

To conclude, we have presented a set of features and a Bayesian computational framework for material category recognition. Our features were chosen to capture various aspects of material appearance in the real world. An augmented LDA (aLDA) framework was designed to select an optimal set of features by maximizing the recognition rate on the training set. We have demonstrated a significant improvement in performance when using our system over the state of the art on the challenging Flickr Materials Database [28]. We have also analyzed the contribution of each feature in our system to the performance gain. Our feature set and computational framework constitute the first attempt at recognizing high-level material categories "in the wild".

References

[1] S. Bae, S. Paris, and F. Durand. Two-scale tone management for photographic look. In *ACM SIGGRAPH*, 2006.

[2] S. Belongie, J. Malik, and J. Puzicha. Shape matching and object recognition using shape contexts. *TPAMI*, 24(4):509–522, 2002.

[3] D. M. Blei, A. Y. Ng, and M. I. Jordan. Latent Dirichlet Allocation. *Journal of Machine Learning Research*, (3):993–1022, 2003.

[4] J. Canny. A computational approach to edge detection. *TPAMI*, 8(6):679–698, Nov 1986.

[5] B. Caputo, E. Hayman, M. Fritz, and J.-O. Eklundh. Classifying materials in the real world. *Image and Vision Computing*, 28(1):150 – 163, 2010.

[6] O. G. Cula and K. J. Dana. Recognition methods for 3d textured surfaces. In *SPIE, Human Vision and Electronic Imaging VI*, pages 209–220, 2001.

[7] N. Dalal and B. Triggs. Histograms of oriented gradients for human detection. In *CVPR*, volume 2, pages 886–893, 2005.

[8] K. J. Dana and S. Nayar. Histogram model for 3d textures. In *CVPR*, pages 618–624, 1998.

[9] K. J. Dana, B. Van-Ginneken, S. K. Nayar, and J. J. Koenderink. Reflectance and texture of real world surfaces. *ACM Transactions on Graphics*, 18(1):1–34, 1999.

[10] P. Debevec, T. Hawkins, C. Tchou, H. P. Duiker, W. Sarokin, and M. Sagar. Acquiring the reflectance field of a human face. In *ACM SIGGRAPH*, pages 145–156, 2000.

[11] R. Dror, E. H. Adelson, and A. S. Willsky. Recognition of surface reflectance properties from a single image under unknown real-world illumination. In *IEEE Workshop on identifying objects across variation in lighting*, 2001.

[12] F. Durand and J. Dorsey. Fast bilateral filtering for the display of high-dynamic-range images. In *ACM SIGGRAPH*, 2002.

[13] L. Fei-Fei and P. Perona. A bayesian hierarchical model for learning natural scene categories. In *CVPR*, volume 2, pages 524–531, 2005.

[14] D. Forsyth and M. M. Fleck. Automatic detection of human nudes. *IJCV*, 32(1):63–77.

[15] M. Fritz, M. Black, G. Bradski, and T. Darrell. An additive latent feature model for transparent object recognition. In *NIPS*, 2009.

[16] H. W. Jensen, S. Marschner, M. Levoy, and P. Hanrahan. A practical model for subsurface light transport. In *ACM SIGGRAPH*, pages 511–518.

[17] J. Koenderink and A. van Doorn. Representation of local geometry in the visual system. *Biological Cybernetics*, 545:367–375.

[18] T. Leung and J. Malik. Representing and recognizing the visual appearance of materials using three-dimensional textons. *IJCV*, 43(1):29–44.

[19] C. Liu, J. Yuen, and A. Torralba. Nonparametric scene parsing: Label transfer via dense scene alignment. In *CVPR*, 2009.

[20] F. Liu and W. Picard. Periodicity, directionality and randomness: Wold features for image modeling and retrieval. *TPAMI*, 18:722–733.

[21] D. G. Lowe. Distinctive image-features from scale-invariant keypoints. *IJCV*, 60(2):91–110, 2004.

[22] S. Marschner, S. H. Westin, A. Arbree, and J. T. Moon. Measuring and modeling the appearance of finished wood. In *ACM SIGGRAPH*, pages 727–734, 2005.

[23] K. McHenry and J. Ponce. A geodesic active contour framework for finding glass. In *CVPR*, volume 1, pages 1038–1044.

[24] F. Nicodemus. Directional reflectance and emissivity of an opaque surface. *Applied Optics*, 4(7):767–775, 1965.

[25] S. Nishida and M. Shinya. Use of image-based information in judgments of surface reflectance properties. *Journal of the Optical Society of America A*, 15:2951–2965.

[26] S. C. Pont and J. J. Koenderink. Bidirectional texture contrast function. *IJCV*, 62(1).

[27] L. Sharan, Y. Li, I. Motoyoshi, S. Nishida, and E. H. Adelson. Image statistics for surface reflectance perception. *Journal of the Optical Society of America A*, 25(4):846–865, 2008.

[28] L. Sharan, R. Rosenholtz, and E. Adelson. Material perception: What can you see in a brief glance? [Abstract]. Journal of Vision, 9(8):784, 2009.

[29] M. Varma and A. Zisserman. A statistical approach to texture classification from single images. *IJCV*, 62(1–2):61–81, 2005.

[30] M. Varma and A. Zisserman. A statistical approach to material classification using image patch exemplars. *TPAMI*, 31(11):2032–2047, 2009.